Supplemental Material

Targeting the m^{6}A RNA modification pathway blocks SARS-CoV-2 and HCoV-OC43 replication

Hannah M. Burgess, Daniel P. Depledge, Letitia Thompson, Kalanghad, Puthankalam Srinivas, Rebecca C. Grande, Elizabeth I. Vink, Jonathan S. Abebe, Wesley P. Blackaby, Alan Hendrick, Mark R. Albertella, Tony Kouzarides, Kenneth A. Stapleford, Angus C. Wilson and Ian Mohr

Supplemental Figures

Supplemental Fig. S1: Validation of siRNAs.

Supplemental Fig. S2: Nuclear accumulation of YTHDF1 and YTHDF3 requires viral RNA synthesis.

Supplemental Fig. S3: Subcellular distribution of host m6A factors unchanged by HCoV-OC43 or SARS-CoV-2 infection.

Supplemental Fig. S4: meRIP-Seq profiling of SARS-CoV-2 and HCoV-OC43 infected cells.

Supplemental Fig. S5: Multiple sites of m6A installation across the SARS-CoV-2 genome are identified by antibody-based immunoprecipitation.

Supplemental Fig. S6: Characterization of METTL3 catalytic inhibitor STM2457 and inactive structural analogue STM2120.

Supplemental Fig. S7: Direct RNA nanopore sequencing of β-coronaviruses.

Supplemental Fig. S8 Interferon response controls.

Supplemental Fig. S9 Protein synthesis rate determination.

Supplemental Tables

Supplemental Table S1, related to Materials and Methods. Oligonucleotide primers used for RT-qPCR.

Supplemental Table S2, related to Materials and Methods. A list of primary antibodies used in this study for immunoblotting and indirect immunofluorescence.

Supplemental Table S3, related to Materials and Methods. A list of siRNAs used to deplete cellular m^{6}A pathway factors.

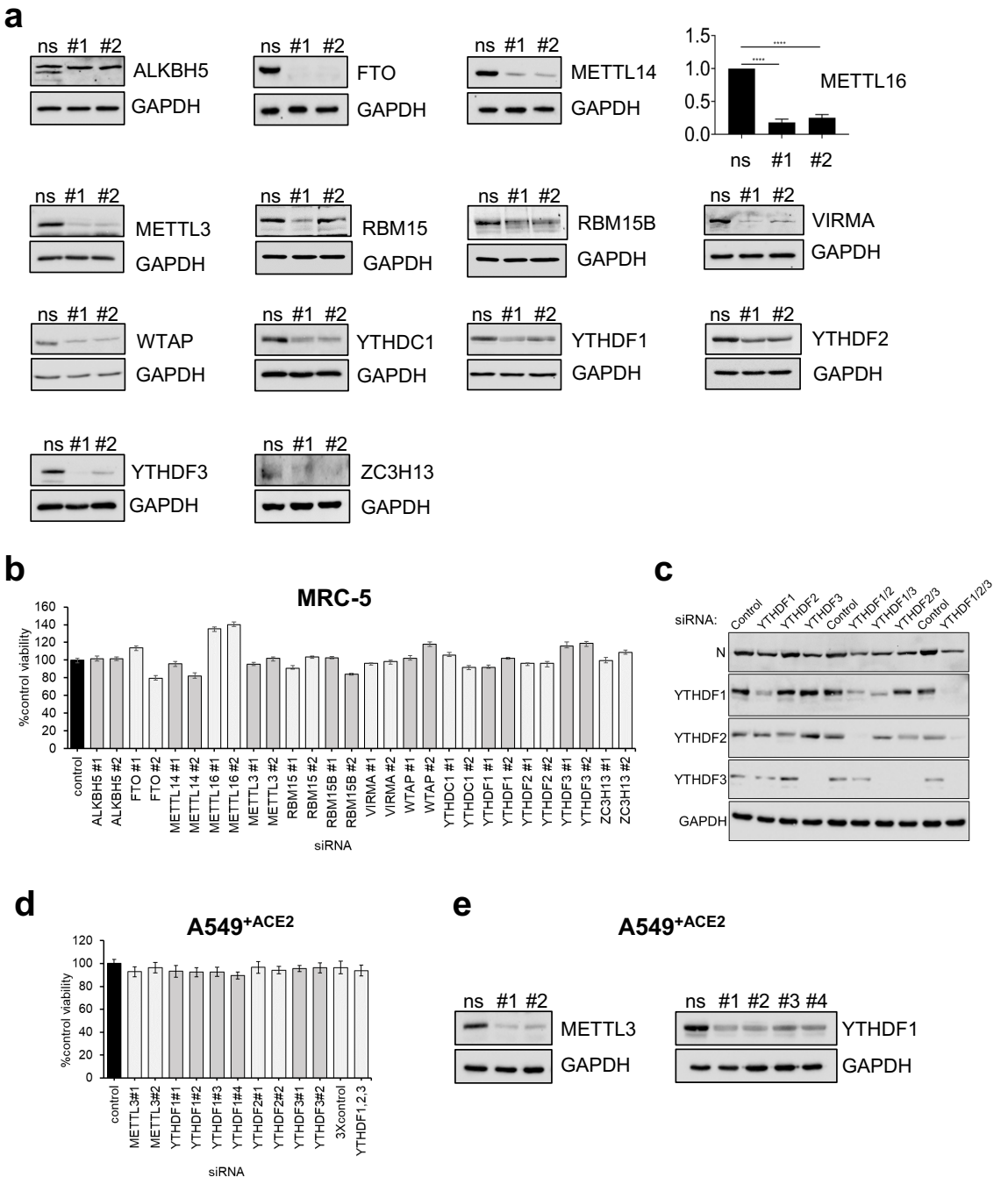

Supplemental Fig. S1: Validation of siRNAs.

a) The extent of depletion for each of the siRNAs used in this study was assessed by immunoblotting. MRC-5 cells were transfected with 20 nM of either the non-silencing control or the targeting RNA as indicated. Whole cell lysates were prepared and probed with antibodies to the targeted polypeptide or to GAPDH (loading control). Lacking a suitable antibody to detect METTL16, depletion of the mRNA was assessed using RT-qPCR and normalized to 18S rRNA, with a significant depletion statistically tested using Students t-test, *** $p<0.001$. **b, d**) The viability of MRC-5 cells (**b**) and A549^{+ACE2} cells (**d**) 72 hours following transfection with siRNAs in used in the infection assays shown in Fig. 1a and c was assessed using a commercial ATP quantitation assay. Each experiment was conducted 3 times with internal duplicates, normalized to control siRNA treated cells and plotted as the mean ± SEM. **c**) High multiplicity HCoV-OC43 infection of MRC-5 cells following transfection with individual siRNAs or combinations of two or three siRNAs. 72 h after siRNA transfection MRC-5 cells were infected with HCoV-OC43 at MOI=3. Lysates were prepared after 24 h and immunoblotted with antibodies to viral nucleocapsid protein (N) or host YTHDF1, YTHDF2 or YTHDF3. GAPDH provides a loading control. **e**) siRNA depletion of METTL3 and YTHDF1 was assessed in A549^{+ACE2} cells as in (a).

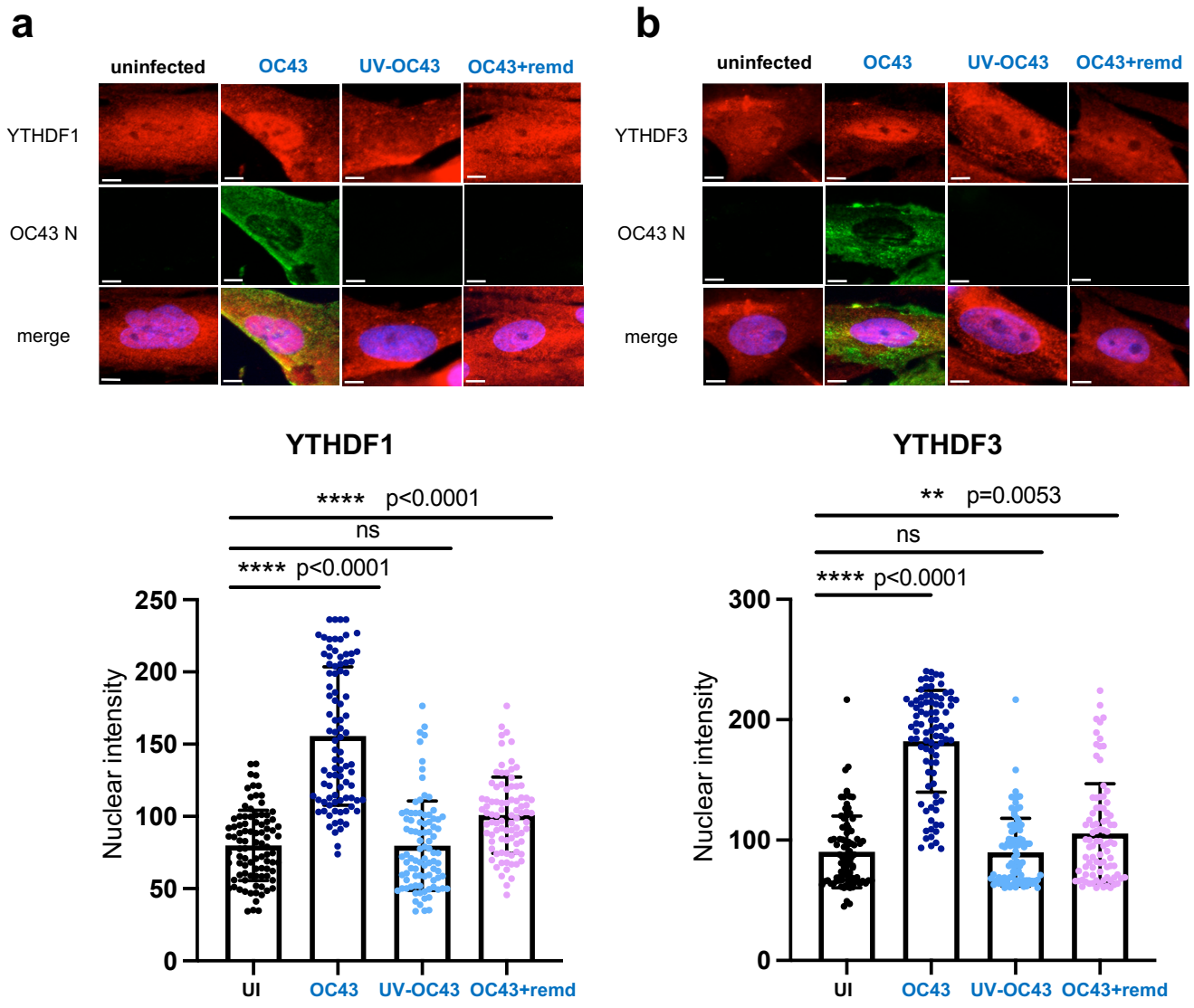

Supplemental Fig. S2: Nuclear accumulation of YTHDF1 and YTHDF3 requires viral RNA synthesis. Indirect immunofluorescence to detect **a**) YTHDF1 or **b**) YTHDF3 in either uninfected MRC-5 cells or MRC-5 infected (24 hpi, MOI=3) with HCoV-OC43 (OC43), UV-inactivated HCoV-OC43 (UV-OC43) or HCoV-OC43 in the presence of the viral RNA-dependent RNA polymerase inhibitor remdesivir (OC43+remd). Simultaneous detection of HCoV-OC43 nucleoprotein (OC43 N) identified cells supporting viral gene expression and the boundaries of the nuclei were identified using DAPI. Scale bar = 10 μm. Quantitation of nuclear signal after normalization to background fluorescence was performed for the YTHDF1 and YTHDF3 primary antibodies. Analysis was performed on ≥100 cells/condition and statistical significance determined using an *F*-test, **** $p \leq 0.0001$, ** $p \leq 0.0047$, ns = not significant.

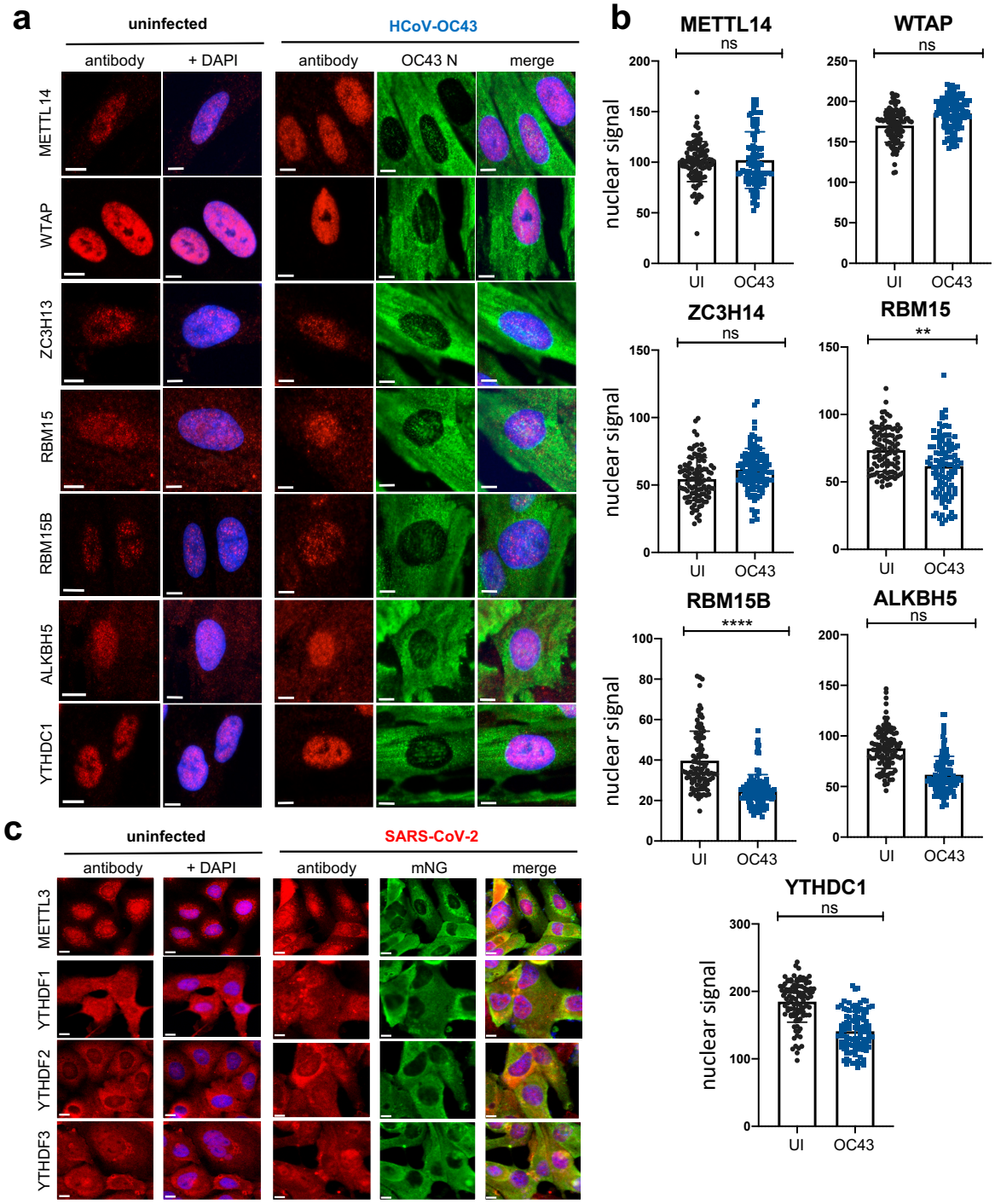

Supplemental Fig. S3: Subcellular distribution of host m^{6}A factors unchanged by HCoV-OC43 or SARS-CoV-2 infection.

a) Indirect immunofluorescence images of representative uninfected or HCoV-OC43 infected MRC-5 cells probed with primary antibodies (red) to nuclear m^{6}A methyltransferase subunits METTL14, WTAP, ZC3H13, RBM15, RBM15B, nuclear m^{6}A binding protein YTHDC1, and nuclear demethylase ALKBH5. Cells were simultaneously probed with an antibody to nucleocapsid (N) protein (green) and counterstained with DAPI (blue). Scale bar = 10 μm. **b**) Quantitation of nuclear signal for each primary antibody used in panel (a) after normalization to background fluorescence. Analysis was performed on ≥100 cells/condition and statistical significance determined using an *F*-test, ** $p \leq 0.01$, *** $p \leq 0.00$, ns = not significant. **c**) Human A549^{+ACE2} cells were infected with SARS-CoV-2 at MOI=1 and cultured for 18 h before being fixed and probed with primary antibodies (red) to METTL3, YTHDF1, YTHDF2 and YTHDF3 and simultaneously imaged for mNeonGreen (mNG) and DAPI (blue). Scale bar = 10 μm.

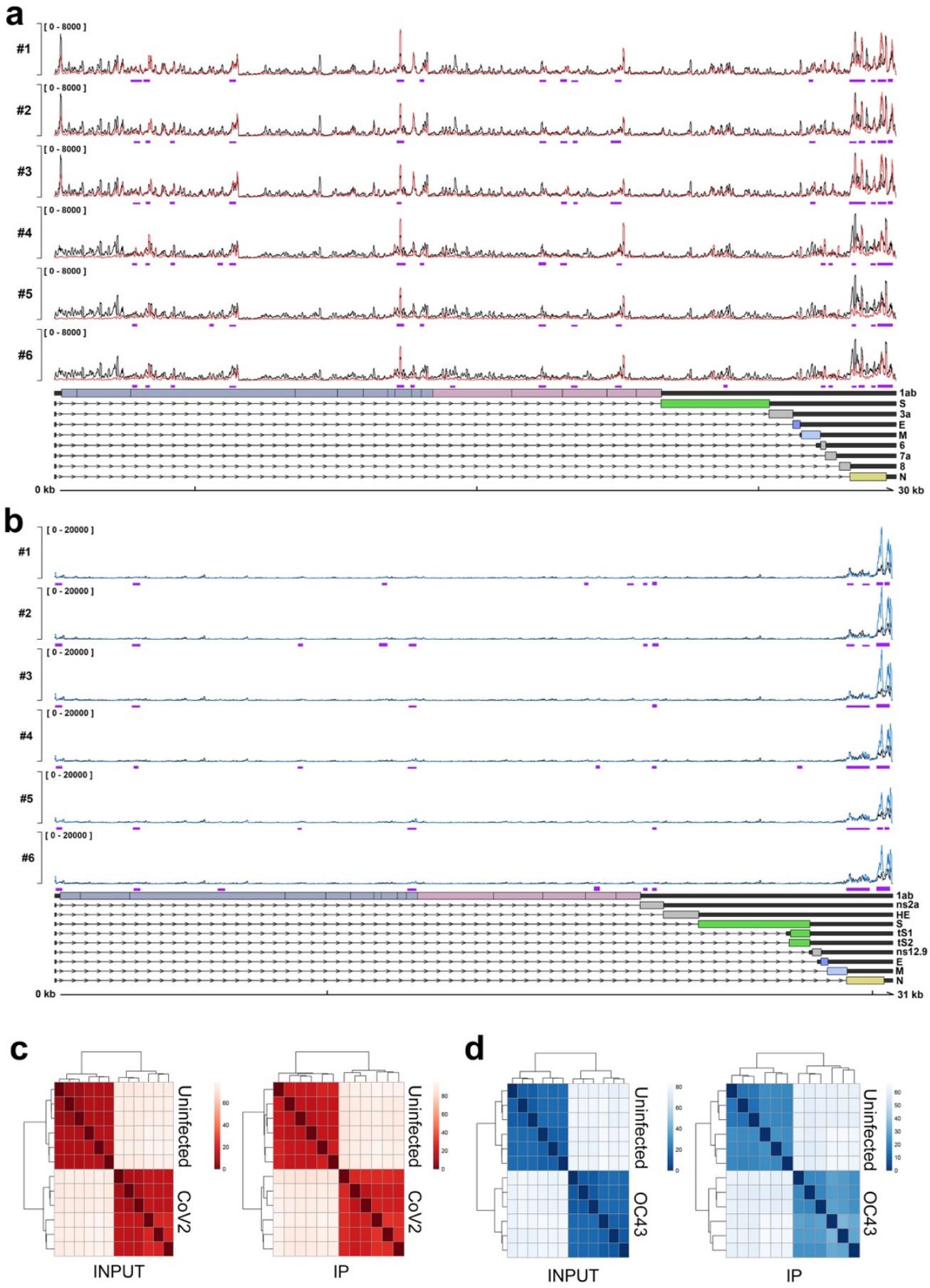
a
[0 - 8000]
#1
#2
#3
#4
#5
#6
1ab
S
3a
E
M
6
7a
8
N
0 kb
30 kb
b
[0 - 20000]
#1
#2
#3
#4
#5
#6
1ab
ns2a
HE
S
tS1
tS2
ns12.9
E
M
N
0 kb
31 kb
c
Uninfected
CoV2
INPUT
IP
d
Uninfected
OC43
INPUT
IP

Supplemental Fig. S4: meRIP-Seq profiling of SARS-CoV-2 and HCoV-OC43 infected cells.
a) Sample distance correlation plots generated by pseudoalignment against the cellular transcriptome of INPUT (left) and m^6A-immunoprecipitation (IP) (right) sequence reads from uninfected and SARS-CoV-2 infected $A549^{+ACE2}$ cells. **b**) Sample distance correlation plots generated by pseudoalignment against the cellular transcriptome of INPUT (left) and IP (right) sequence reads from uninfected and HCoV-OC43 infected MRC-5 cells. **c**) Six biological replicates of $A549^{+ACE2}$ cells were infected at MOI=0.1 for 48 h. meRIP was performed on total RNA with rRNA-depleted sequencing libraries prepared from the INPUT (black lines) and IP (red lines) fractions. Normalization was performed across all datasets by randomly subsampling 500,000 SARS-CoV-2-aligned read pairs prior to the generation of coverage plots that span the whole genome. **d**) Six biological replicates of MRC-5 cells were infected at MOI=3 for 24 h. meRIP-seq was performed on total RNA with rRNA-depleted sequencing libraries prepared from INPUT (black lines) and IP (red lines) fractions. Normalization was performed across all datasets by randomly subsampling 200,000 HCoV-OC43-aligned read pairs prior to the generation of coverage plots that span the whole genome. For all datasets, peak-calling was performed using MACS2 (Zhang et al. 2008) to and regions significantly enriched ($q < 0.05$) in meRIP-Seq datasets are shown by purple bars with the height of the bar denoting the strength of enrichment. The y-axis denotes read depth while x-axis denotes genome co-ordinate. Transcript boundaries, UTRs (narrow boxes), and coding sequences (wide boxes) were derived using StringTie2 (Kovaka et al. 2019) from nanopore direct RNA sequencing datasets (Supplemental Fig. S7).

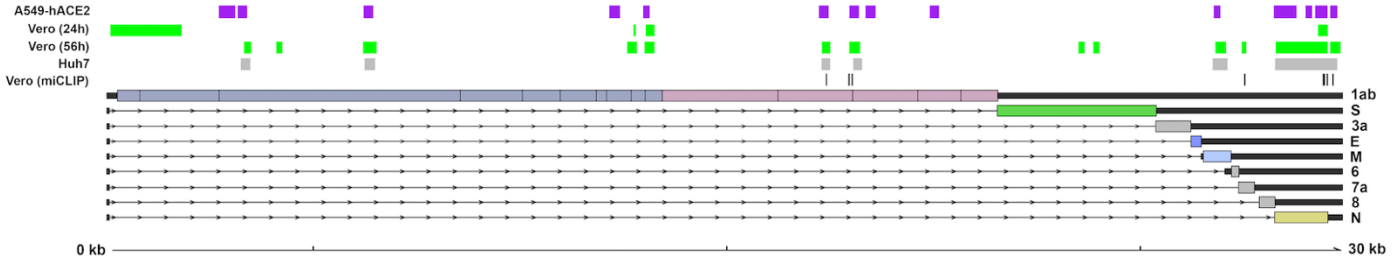

Supplemental Fig. S5: Multiple sites of m^{6}A installation across the SARS-CoV-2 genome are identified by antibody-based immunoprecipitation.

Schematic showing the SARS-CoV-2 genomic and eight major sub-genomic RNAs, each labeled according to the principal translation product. The fourteen high-confidence meRIP-Seq peak regions identified in the study are shown as purple boxes. meRIP-Seq peaks reported by Liu and colleagues (Liu et al. 2021) using RNA from SARS-CoV-2 infected African green monkey Vero cells collected at 24 hpi or 56 hpi (in green) and human hepatocarcinoma cell line Huh7 (in gray). Eight candidate sites identified by miCLIP on infected Vero cell RNA at 56 hpi are show as vertical lines.

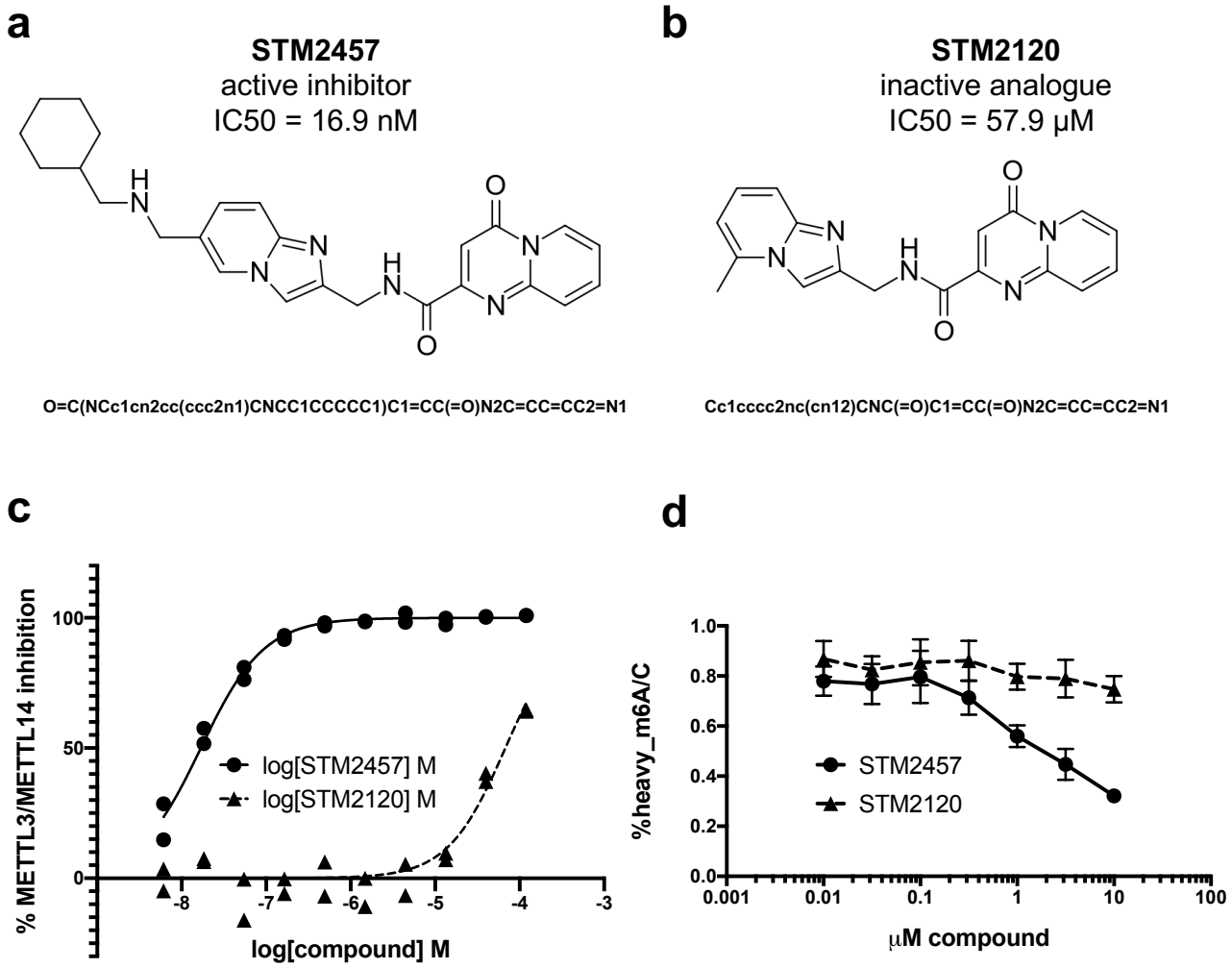

Supplemental Fig. S6: Characterization of METTL3 catalytic inhibitor STM2457 and inactive structural analogue STM2120.

a) Chemical structure and simplified molecular-input line-entry system (SMILES) representations of the active METTL3 inhibitor STM2457. **b**) Chemical structure and SMILES representations of control compound STM2120. **c**) Rapid Fire Mass Spectrometry (RFMS) enzymatic assay showing inhibition of the METTL3/14 enzyme complex using a dose range of STM2457 and STM2120. The IC50 values extrapolated from this experiment are: STM2457 = 16.9 nM and STM2120 = 67.8 µM. **d**) Cellular m^6A reduction assay by heavy methionine labeling RNA-mass spectrometry analysis of poly(A) RNA isolated from Kasumi-1 acute myeloid leukemia cells after 16 h treatment with a dose range of STM2457 or STM2120.

a

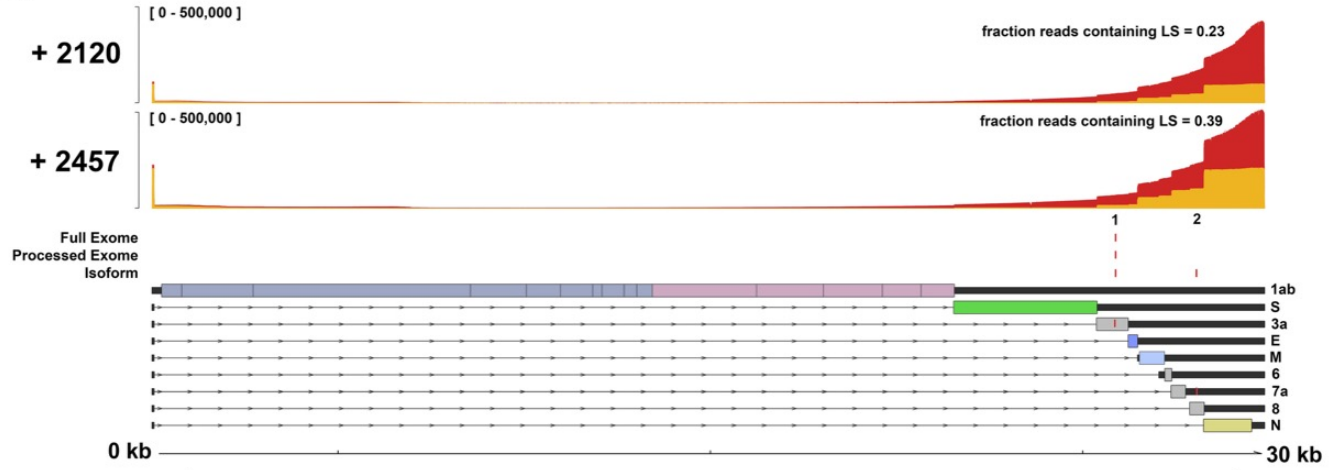

Candidate	Confidence	Position	DRUMMER			Eligos2	nearest AC	11-mer	homopolymer
			Full Exome	Processed Exome	Isoform				
1	low	25,882	0.03	0.03	0.03		0	GTGTAACTTCT	
2	very low	28,052			0.01	0.01	-6	AGAAAATCAGC	TRUE

very low	observed in only one analysis + error profile < 0.1
low	observed in only one analysis + error profile ≥ 0.1 || observed in multiple analyses + error profile < 0.1
medium	observed in multiple analyses (same tool) + error profile > 0.1
high	observed in multiple analyses (multiple tools) + error profile < 0.1
very high	observed in multiple analyses (multiple tools) + error profile > 0.1

b

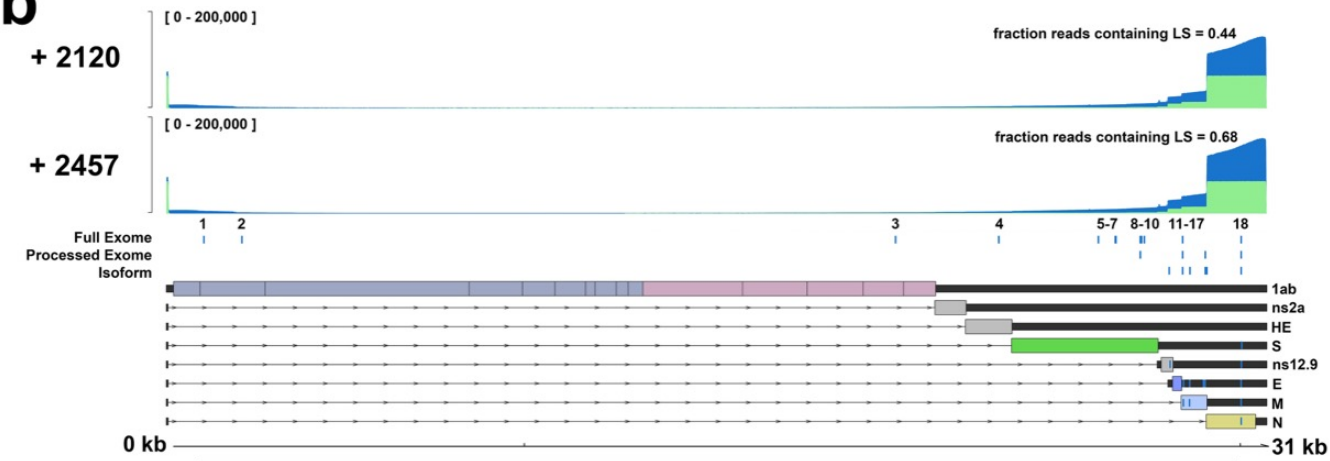

Candidate	Confidence	Position	DRUMMER			Eligos2	nearest AC	11-mer	homopolymer
			Full Exome	Processed Exome	Isoform				
1	very low	1,055	0.03				-7	GCATTATTTCC	TRUE
2	low	2,116	0.09				14	GAATTCTAAGA	
3	low	20,376	0.10				3	TGACTCCAGCA	
4	very low	23,261	0.06				1	CATGACGGCGG	
5	very low	26,037	0.02				6	CTATAGGTAAT	
6	very low	26,509	0.03				14	AGAAAATCAGA	TRUE
7	very low	26,530	0.02				4	CACTTTGGCTG	TRUE
8	low	27,209	0.08	0.08			1	ATGTACACTGG	
9	very low	27,244	0.02				1	TATAACTGAAA	TRUE
10	very low	27,322	0.02				-1	TTCAATACCCA	TRUE
11	low	28,015			0.10		-5	AAATGGTTTCA	TRUE
12	low	28,259				0.10	1	TAATACCTTAG	
13	very high	28,390	0.10	0.10	0.11	0.11	1	TAAAACTACAC	TRUE
14	low	28,550				0.12	-22	ATTATTTTGTG	TRUE
15	very low	28,593			0.05		9	TTTTCAATTGC	TRUE
16	low	29,024		0.02	0.02		5	ACCCAAAAGGG	TRUE
17	very low	29,066			0.02		-22	AATATCTAAAT	TRUE
18	very high	30,024	0.16	0.17	0.17	0.19	1	CAGAACTCGCA	

very low	observed in only one analysis + error profile < 0.1
low	observed in only one analysis + error profile ≥ 0.1 || observed in multiple analyses + error profile < 0.1
medium	observed in multiple analyses (same tool) + error profile > 0.1
high	observed in multiple analyses (multiple tools) + error profile < 0.1
very high	observed in multiple analyses (multiple tools) + error profile > 0.1

Supplemental Fig. S7: Direct RNA nanopore sequencing of β-coronaviruses.
Direct RNA Sequencing (DRS) libraries were prepared from **a**) SARS-CoV-2 infected $A549^{+ACE2}$ cells, and **b**) HCoV-OC43 infected MRC-5 cells, treated with 30 μM METTL3 inhibitor STM2457 or non-inhibiting control STM2120. Coverage plots generated using the full dataset (used for Full Exome analysis) for each sample is shown in red or blue while filtering to retain only sequences containing the 5' leader sequence (LS) resulted in the purple coverage plots (used for Processed Exome and Isoform levels analyses). gRNA and sgRNAs are shown below and ORFs that are conserved between SARS-CoV-2 and HCoV-OC43 colored identically. Putative m^6A modification (candidate) sites identified by DRUMMER are labelled within the respective figure panels and are detailed in the table below. The values shown for each candidate site, at each level of analysis (Full Exome, Processed Exome, Isoform) using DRUMMER and a similar analysis of the Full Exome using ELIGOS2 (Jenjaroenpun et al. 2021), represent the fractional difference in base call error-rate at the given position – note that values are only presented for candidate sites tested as significant. Nearest AC indicates (in nt) the closest AC dinucleotide while the 11-mer column shows the candidate site (center) in its local sequence context with putative DRACH motifs identified in red text. The homopolymer column indicates whether a homopolymer > 2nt is located within or partially overlaps with the 11-mer sequence. A confidence measure is applied to each candidate site based on whether it is detected across multiple comparisons/tools and the difference observed in base call error-rate.

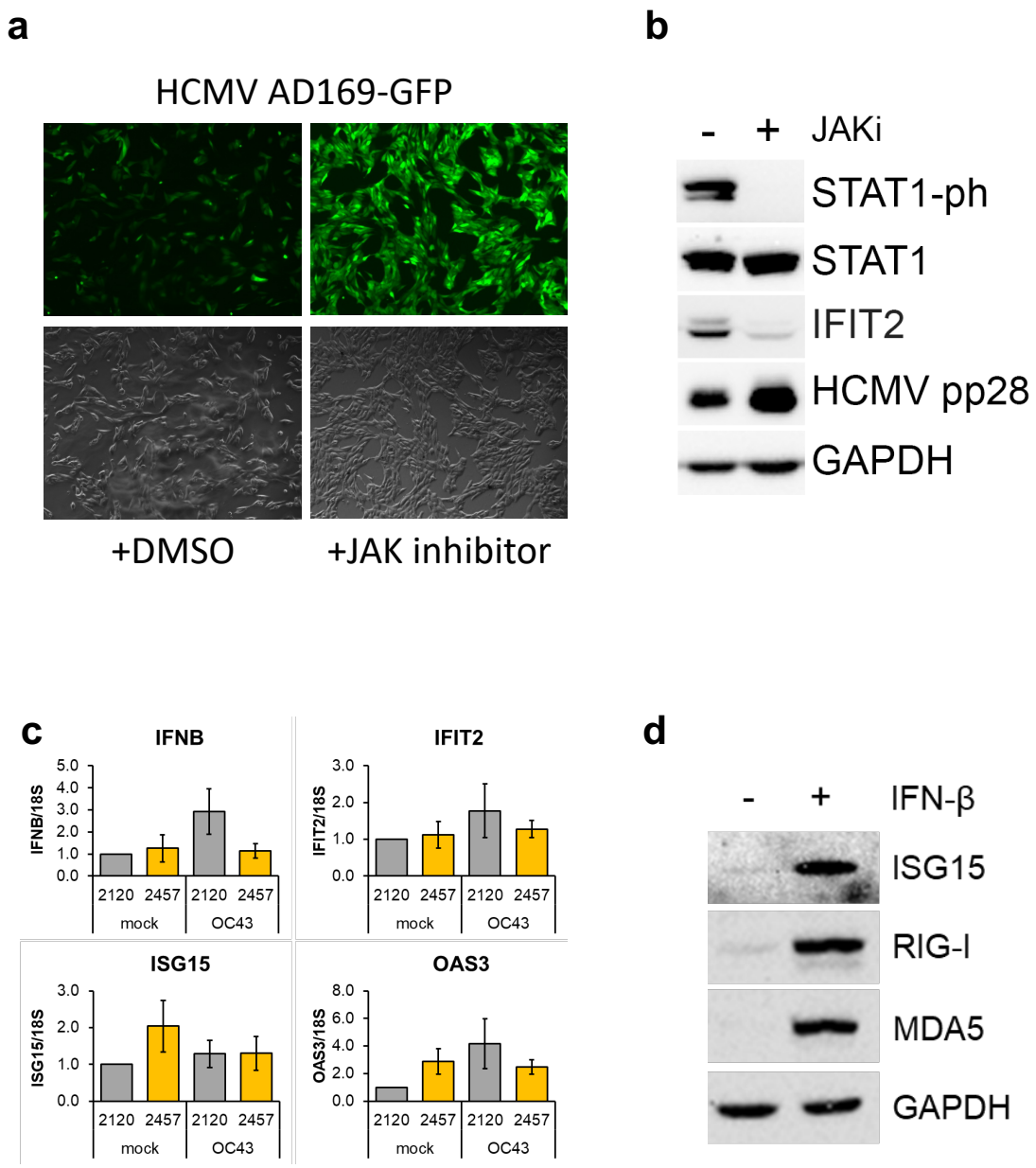

Supplemental Fig. S8 Interferon response controls.
a) Normal human dermal fibroblasts (NHDFs) were infected with GFP-HCMV Ad169 at MOI=0.05 in the presence of 10μM JAK inhibitor (pyridone 6) or vehicle control (DMSO) and imaged for GFP fluorescence and phase contrast at 4 days post infection. **b**) The same cells were lysed and subject to immunoblotting for JAK-target phospho(Y701)-STAT1 (Cell Signaling; 9171), total STAT1 (Cell Signaling; 9172), HCMV protein pp28 (Virus Sys; CA004-100), interferon stimulated gene (ISG) IFIT2 (Proteintech; 12604-1-AP) and GAPDH. **c**) cDNA from Fig 5c (MRC-5 24 hpi HCoV-OC43 MOI=3 treated with 30μM 2120/2457) was subject to additional qRT-PCR for IFNB and ISGs IFIT2, OAS3 and ISG15 as indicated, normalized to control compound treated mock-infected cells and presented as the ± SEM (n=4). **d**) MRC-5 cells were treated with 100 units/ml human interferon β (PBL Assay Science; #11415-1) for 24 hours and lysates immunoblotted for ISGs MDA5, RIG-I and ISG15 as indicated.

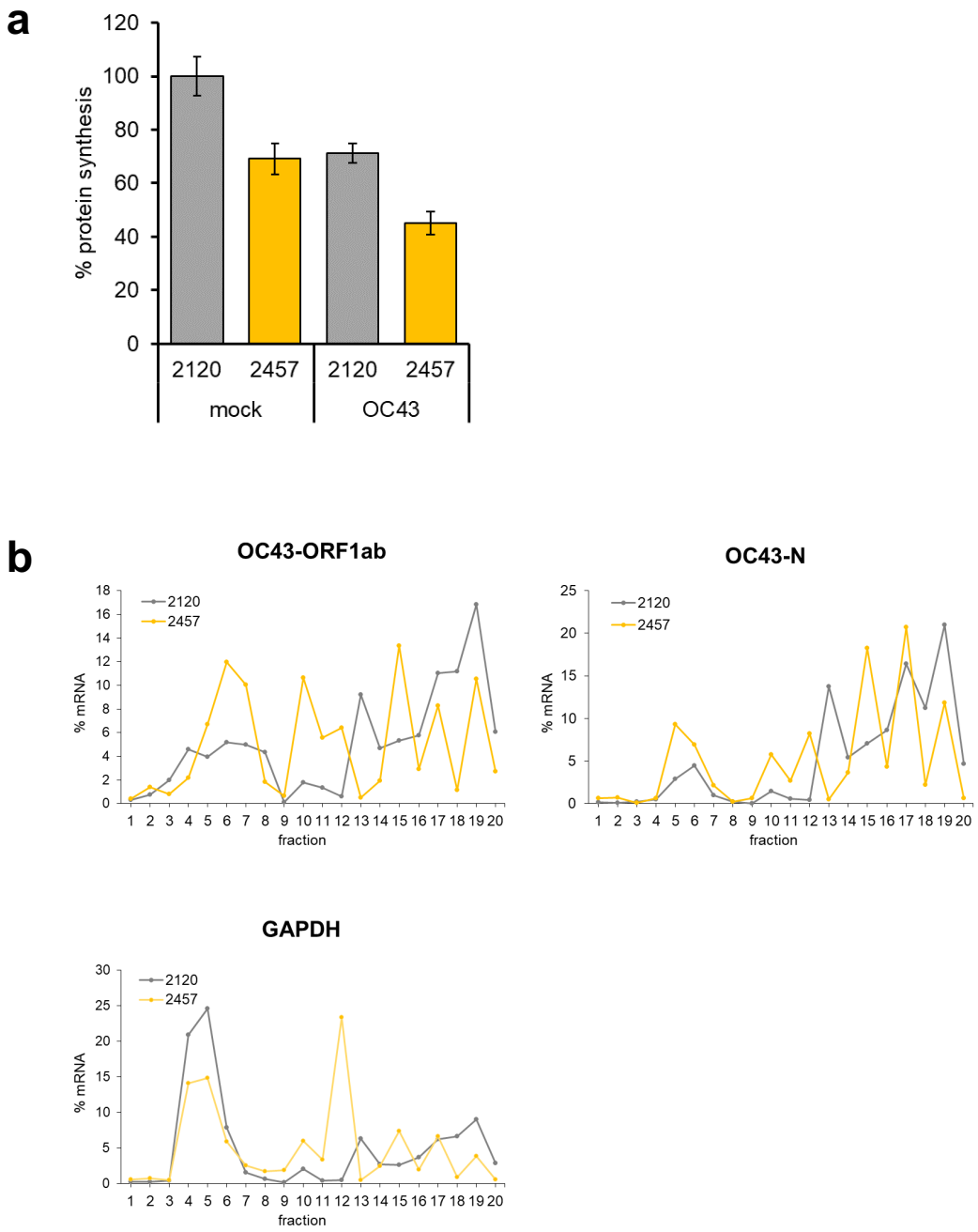

Supplemental Fig. S9 Protein synthesis rate determination

a) Total protein synthesis rates of MRC-5 cells infected with HCoV-OC43 at MOI=3 in the presence of 30 μM STM2120 or STM2457 as shown in Fig. 5d were measured by liquid scintillation counting of ^{35}S-incorporated into TCA-precipitated proteins as in (Burgess and Mohr 2015). Values are the means of 3 biological replicates and are normalized to control compound STM2120-treated mock infected samples ± SEM. **b**) The relative abundance of full-length viral genomic (ORF1a/b) and ORF N sub-genomic RNAs and host GAPDH mRNA in each gradient fraction was determined by RT-qPCR from fractions shown in Fig. 5 from HCoV-OC43 infected MRC-5 cells treated with STM2120 (grey) or STM2457 (yellow).

LITERATURE CITED

Burgess HM, Mohr I. 2015. Cellular 5“-3” mRNA exonuclease xrn1 controls double-stranded RNA accumulation and anti-viral responses. *Cell Host Microbe* **17**: 332–344. doi:10.1016/j.chom.2015.02.003.

Jenjaroenpun P, Wongsurawat T, Wadley TD, Wassenaar TM, Liu J, Dai Q, Wanchai V, Akel NS, Jamshidi-Parsian A, Franco AT, et al. 2021. Decoding the epitranscriptional landscape from native RNA sequences. *Nucleic Acids Res* **49**: e7. doi:10.1093/nar/gkaa620

Kovaka S, Zimin AV, Pertea GM, Razaghi R, Salzberg SL, Pertea M. 2019. Transcriptome assembly from long-read RNA-seq alignments with StringTie2. *Genome Biol* **20**: 278–13. doi:10.1186/s13059-019-1910-1

Liu J, Xu Y-P, Li K, Ye Q, Zhou H-Y, Sun H, Li X, Yu L, Deng Y-Q, Li R-T, et al. 2021. The m6A methylome of SARS-CoV-2 in host cells. *Cell Res* 1–11. doi:10.1038/s41422-020-00465-7

Zhang Y, Liu T, Meyer CA, Eeckhoute J, Johnson DS, Bernstein BE, Nusbaum C, Myers RM, Brown M, Li W, et al. 2008. Model-based analysis of ChIP-Seq (MACS). *Genome Biol* **9**: R137–9. doi: 10.1186/gb-2008-9-9-r137.